19th Brazilian Congress of Thermal Sciences and Engineering
November 06th-10th, 2022, Bento Gonçalves - RS - Brazil

ENC-2022-0260
STEADY-STATE SIMULATION OF THE AIR-CONDITIONING SYSTEM OF A HYBRID VEHICLE

Leonardo Toigo Caron
Christian Johann Losso Hermes
POLO Labs, Departament of Mechanical Engineering, Federal University of Santa Catarina, Florianópolis, SC, Brazil
leonardo.caron@polo.ufsc.br

Diogo Lôndero da Silva
Laboratory of Vehicular Refrigeration - Federal University of Santa Catarina, Joinville, SC, Brazil

Abstract. *The development and commercialization of hybrid and electric vehicles have been drastically increased over the past years. This new endeavor presents several benefits, such as the reduction of direct emission of polluting gases, but also brings challenges related to the efficient use of energy stored in batteries. Among the different subsystems present in hybrid vehicles, the climate control system has a very significant effect on energy consumption. For this reason, the main purpose of this paper is to develop a steady-state mathematical model for an automotive air conditioning system, and use it to identify energy efficiency opportunities. The heat exchangers have been modeled based on a distributed approach, according to which each tube of the heat exchanger was divided into nonoverlapping control volumes. Heat transfer, for each element, is calculated considering average properties among inlet and outlet conditions, and the total heat transfer is the sum up of those calculated at each control volume. The compressor model is based on semi-empirical equations, where data from a compressor catalogue was used to determine the fitting coefficients. In order to simulate the AC system cooling mode, both condenser subcooling and evaporator superheating were imposed while an isenthalpic expansion device was considered. Based on geometric input data to heat exchangers, such as total heat transfer area and refrigerant circuitry, a Newton-like method is used iteratively to obtain the output parameters. Mathematical convergence is obtained when the heat transferred in heat exchangers are equal to the heat calculated over the refrigeration loop with superheating and subcooling degrees imposed. As a result, the model comes out with the heat exchanger temperature profile and heat duty, the working pressures, the compressor power and the coefficient of performance (COP). The simulations results show that a decrease in the compressor speed from 6000 rpm to 3000 rpm increases the COP by approximately 50%. In addition, it was observed that the latent heat load exceeds the sensible one when the air dry-bulb temperature is 35°C and the relative humidity exceeds 55%, considering the SAE J2765 L35 conditions.*

Keywords: *automotive air-conditioning, vapor compression refrigeration, hybrid vehicle, system simulation*

1. INTRODUCTION

The commercialization of electric and hybrid vehicles has increased in recent years, being accompanied by technological development and energy regulations associated with this new segment (IEA, 2022). Although different technologies are already available, there is a consensus that electric efficiency and battery range extension are mandatory for the competitiveness of this new platform in relation to internal combustion vehicles.

Besides providing passenger thermal comfort and safety requirements, the air conditioning system in hybrid and electric vehicles represents a significant amount on energy consumption, therefore, reducing battery range and mileage operation. Depending on the size of air-conditioning system and the driving pattern, an average of 30-40% decrease in driving range can occur (Farrington and Rugh, 2000; Lee *et al.*, 2013).

Although the requirements of an air conditioning system for electric and conventional vehicles are the same, there are differences between its basic design concepts. In a conventional vehicle, a belt driven compressor is commonly coupled with the engine, thus being dependent on the engine speed. Therefore, the compressor of the air conditioning system may operate on a higher speed when a low cooling demand is necessary. On the other hand, a compressor driven by DC electricity is generally used in hybrid vehicles, allowing its speed to be controlled by a frequency inverter. It is also

observed that swash-plate type compressors are generally applicable to conventional vehicles, while scroll compressors are more suitable for hybrid vehicles (Zhang *et al.*, 2018).

In order to meet the energy efficiency requirements of the electric car air conditioning system, intensive research and development activities have been required (Liang *et al.*, 2021). One way to reduce the time and cost of these activities is the use of mathematical models capable of simulating the energy performance of the air conditioning system. Ko *et al* (2021) developed a transient simulation integrated with the air handling unit and cabin model aiming at evaluating the effect of the system start-up and cabin pull-down under various thermal load conditions on the power consumption. Feng and Hrnjak (2016) presented an experimental and numerical analysis of the air conditioning system with a heat pump cycle, and evaluated heating and cooling capacity in order to figure out the effect of the refrigerant charge imbalance between cooling and heating modes. Da Silva and Cordoba (2017) developed a steady-state simulation model for an AC system for a conventional vehicle, which was employed to investigate the effect of evaporator air flow rate and refrigerant charge on the overall performance.

Although the literature review presents mathematical models for the simulation of air conditioning systems, relatively few studies were applied to hybrid vehicles. For this reason, this work is aimed at developing a steady-state simulation model for the air-conditioning system for a hybrid vehicle. The proposed model is able to predict the temperature profiles and heat duties of the heat exchangers, the working pressures, the compressor power and the coefficient of performance (COP).

2. AIR CONDITIONING SYSTEM DESCRIPTION

In comparison with conventional vapor cycle systems for vehicular air conditioning applications, the key difference concerning hybrid vehicles lies on the compressor power supply. Generally, the main source of power supply comes from the vehicle battery, compressor speed is controlled by an integrated inverter in the compressor body and might be set to a proper value depending on cooling demand. Figure 1a shows a simplified overview of an air conditioning system, the cycle structure is composed by four different components: (i) compressor, (ii) condenser, (iii) throttling device and (iv) evaporator. The corresponding thermodynamic cycle is presented in Figure 1b, where the continuous and doted lines compares an ideal and real processes, respectively. The process starts on state (1), where low pressure refrigerant enters the compressor chamber and is compressed to the high-pressure side (2), in this process the refrigerant temperature is increased while electric power is consumed by the compressor. High temperature and high-pressure refrigerant, then, enters the condenser and transfer heat to the surroundings, reducing its enthalpy and leaving the condenser as liquid (3). From the condenser exit, the refrigerant flow enters the throttling device, reducing is pressure on an ideal isenthalpic process (4). The main differences of the real process represented in Figure 1 bare the fluid refrigerant pressure drop in the heat exchangers and the presence of superheating and subcooling on states (1) and (3). Finally, in the evaporator, air transfer heat to the evaporating two-phase refrigerant flow, increasing refrigerant enthalpy and leaving the evaporator the cycle starts again. It must be noted that, on the evaporator, sensible and latent heat transfer occurs from the air, reducing not only temperature but also its humidity ratio (Stoecker, 1998).

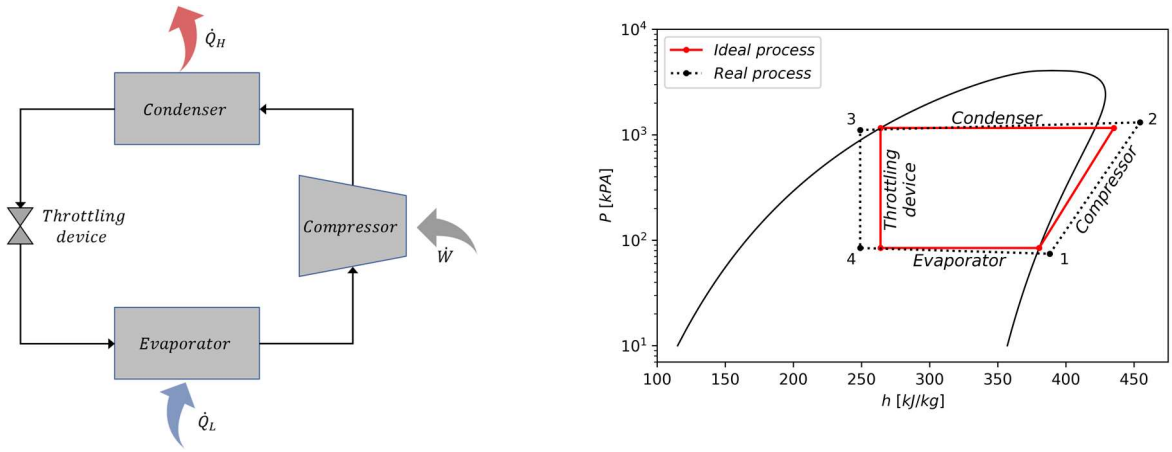

(a) Air conditioning cycle (b) Pressure – enthalpy diagram

Figure 1 - Air conditioning system

3. MATHEMATICAL MODEL

In order to simulate the thermodynamic cycle and its components, a few assumptions were considered: (i) steady-state simulation, (ii) isenthalpic expansion device, (iii) semi-empirical correlations for compressor volumetric efficiency and power consumption, (iv) superheating and subcooling imposed.

3.1 Compressor

A semi-empirical correlation for the compressor volumetric efficiency and power consumption presented by Li (2013) was used in the simulation. Also, an electric driven compressor datasheet was considered to determine the fitting coefficients for the model. The following equation was used to determine the volumetric efficiency:

$$\eta_{v,ref} = b_1 + b_2\left(\left(\frac{P_d}{P_s(1-dp)}\right)^{1/k}\right) \tag{1}$$

Where $\eta_{v,ref}$ is the volumetric efficiency at a specified speed, P_d the discharge pressure, P_s the suction pressure, dp the pressure drop inside the compressor, b_1 and b_2 the fitting coefficients. Compressor power consumption is described by the following equation:

$$W_{ref} = P_s\dot{V}_s a_1\left[\left(\frac{P_d}{P_s}\right)^{a_2+\frac{k-1}{k}} + \frac{a_3}{P_d}\right] + W_{loss} \tag{2}$$

Where P_s is the suction pressure, $\dot{V}_s$ the displacement rate, k the isentropic coefficient, W_{ref} the compressor power consumption at a specified speed, W_{loss} the constant loss due to electro-mechanical and the fitting coefficients represented as a_1, a_2 and a_3. For different compressor speed a polynomial equation was adjusted by the author, resulting in the following equations for the volumetric efficiency and compressor power consumption:

$$\frac{\eta_v}{\eta_{v,ref}} = d_1 + d_2\left(\frac{N}{N_{ref}}\right) + d_3\left(\frac{N}{N_{ref}}\right)^2 \tag{3}$$

$$\frac{W_{cp}}{W_{ref}} = \frac{N}{N_{ref}}\frac{\eta_v}{\eta_{v,ref}}\left\{e_1 + e_2\left(\frac{N}{N_{ref}}\right) + e_3\left(\frac{N}{N_{ref}}\right)^2\right\} \tag{4}$$

3.2 Condenser

A discrete model was considered in the condenser mathematical modeling, where the outlet condition of a control volume is the inlet condition for the following control volume. Average properties of the refrigerant and air were also considered during the heat transfer analysis. To determine the total heat transfer of each control volume, the effectiveness-NTU method was considered (Shah, Ramesh K and Sekulic, 2003), where the following equations were used:

$$\dot{Q} = \varepsilon\dot{Q}_{max} \tag{5}$$

$$\varepsilon = 1 - exp\left(-\frac{NTU^{0.22}}{C_r}(exp(-C_r NTU^{0.78}) - 1)\right) \tag{6}$$

Fin efficiency and surface efficiency were also considered into the analysis, the method is briefly described by Shah and Sekulic (2003).

For each fluid, an energy balance can be obtained, resulting in the following equations:

$$\dot{Q}_{cond} = \dot{m}_r(h_{r,in} - h_{r,out}) \tag{7}$$

$$\dot{Q}_{cond} = \dot{m}_{air}(h_{air,out} - h_{air,in}) \tag{8}$$

Table 1 summarizes the correlations used in the numerical model for the heat transfer and friction factor coefficient.

Table 1 – Air and refrigerant correlations

Air side correlations	
Colburn factor	(Chang and Wang, 1997)
Friction factor coefficient	(Chang *et al.*, 2000)
Refrigerant correlation – vapor and liquid region	
Heat transfer coefficient	(Petukhov, 1970)
Pressure drop	(Churchill, 1977)
Refrigerant correlation – two-phase region	
Heat transfer coefficient	(Shah, Mirza M., 2016)
Pressure drop	(Kim and Mudawar, 2013)

3.3 Evaporator

While on the air side of the condenser only sensible heat transfer occurs, latent heat transfer due to the vapor condensation in the air might take place on the evaporator. To consider this part of the heat analysis, an equivalent dry bulb temperature approach developed by Wang and Hihara (2003) was considered, the model was validated with temperatures between 22 and 36 °C, relative humidity from 20 to 75 % and Reynolds number between 500 and 4000. The results predicted both cooling capacity and vapor condensate with a deviation lower than 10 %.

With the inlet equivalent dry bulb temperature, the mathematical analysis uses the same set of equations as the condenser to obtain the heat transfer for each control volume, despite using moist air thermodynamic properties. The total heat is the sum up of both sensible and latent portion:

$$\dot{Q}_{evap} = \dot{Q}_{sen} + \dot{Q}_{lat} \tag{9}$$

It can also be described in terms of the thermodynamic properties involved in the process:

$$\dot{Q}_{evap} = \dot{m}_{air} c_{p,air} \left(T_{air,in} - T_{air,out}\right) + \dot{m}_{air} h_{lv} (\omega_{air,in} - \omega_{air,out}) \tag{10}$$

3.4 Simulation procedure

In order to simulate the air-conditioning system, two more equations are necessary to solve for the working pressures. These equations are the global mass balance and the equality among compressor and expansion valve mass flow. It is known that the inclusion of these equations might carry out numerical instability (Gonçalves *et al.*, 2009), to overcome such issue the condenser subcooling and evaporator superheating were imposed into the analysis. With this assumption, the outlet refrigerant enthalpy for each heat exchanger can also be determine and the following set of equations are included into the model

$$\dot{Q}_H = \dot{m}_r [h_{r,in} - h_{r,out}(\Delta T_{sc})] \tag{11}$$

$$\dot{Q}_L = \dot{m}_r [h_{r,out}(\Delta T_{sh}) - h_{r,in}] \tag{12}$$

The solutions of the pressure distribution on the evaporator and the condenser are obtained when Eqs. (11) and (12) converge to the same result as Eqs. (7) and (10), respectively. The algorithm procedure is described in Figure 2.

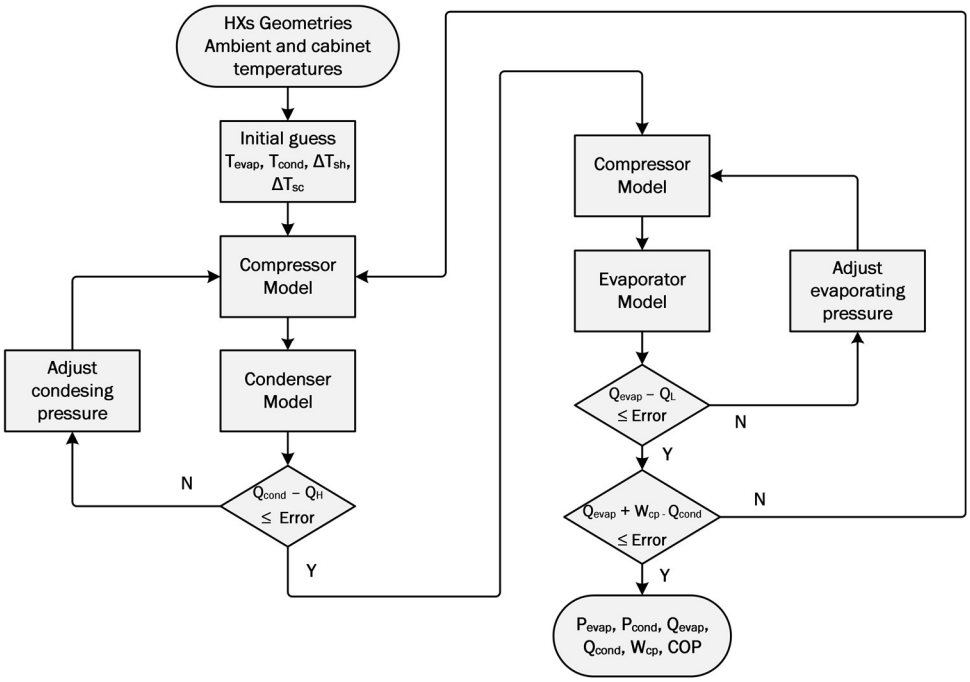

Figure 2 - Algorithm procedure

4. RESULTS

Data from the compressor catalogue was used to determine the fitting coefficients for Eqs (1) to (4). The catalogue available only provided cooling performance and COP values, power consumption values were then calculated based on each set of data. Due to a lack of power consumption data, the W_{loss} value was set to zero, therefore, the entire power available to the compressor was used during the compression phase and no mechanical nor heat loss were considered. The fitting coefficients are presented in Table 2.

Table 2 - Fitting coefficients

Variable	*Value*	*Variable*	*Value*
a_1	0.4131	b_1	1.0629
a_2	0.8938	b_2	−0.0421
a_3	1.9556e06	dp	0
W_{loss}	0	d_1	0.8279
e_1	1.2549	d_2	0.2761
e_2	−0.3159	d_3	−0.0993
e_3	0.1340	−	−

A good agreement between the fitted equation and the experimental data was obtained, for the mass flow all the calculated values were within ±10 % error band and for the compressor power 76 % of the data were within ±10 %. Figure 3a shows the predicted mass flow rate while Figure 3b presents the compressor power consumption.

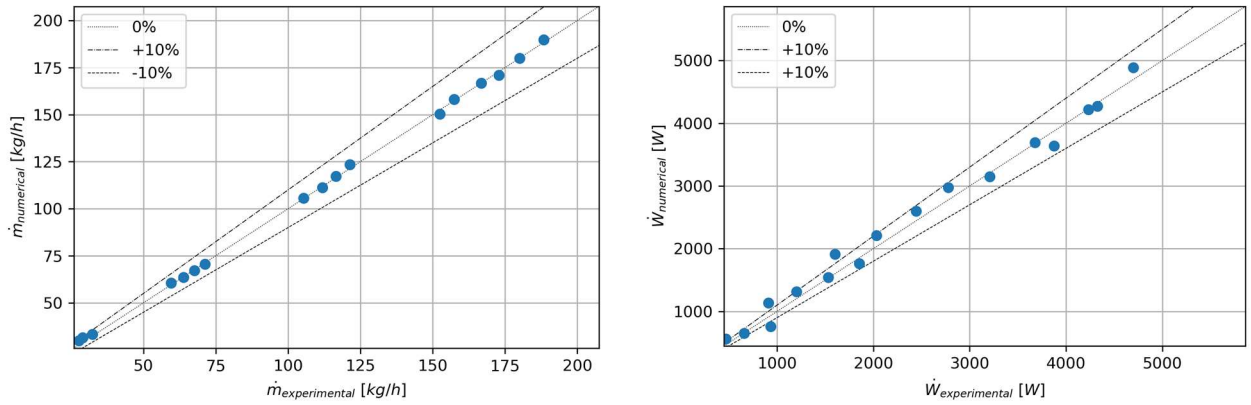

(a) Mass flow rate (b) Power consumption

Figure 3 – Comparison among compressor experimental and numerical data

The analyses were performed considering the SAE J2765 (2017) technical standard that establishes procedures to determine system COP on a test bench, the document also specifies inlet air conditions for different test configurations. Otherwise specified, the analyses below considered the parameters listed in Table 3.

Table 3 – Simulation parameters

Parameter	***Value***
Ambient temperature	35 °C
Compressor speed	1800 rpm
Condenser air inlet temperature	35 °C
Condenser air face velocity	2 m/s
Evaporator air inlet temperature	35 °C
Evaporator air inlet humidity	40 %
Evaporator air mass flow	9 kg/min
Target air temperature downstream evaporator	3 °C

Figure 4 shows the sensibility of the mathematical model to the number of elements used to discretize the heat exchangers. It is known that a low number of elements can lead to poor results besides providing a faster simulation run time, while a large number of elements proceed to better results although a higher run time occur. Figure 4a presents the deviation of the heat exchanger heat duty and compressor power on the system performance, for a low number of elements per tube a higher deviation is obtained although not being a significant deviation in terms of absolute value. Figure 4b shows the working pressure deviation, it can be noted that the condensing pressure is more susceptible to variations due to the number of elements per tube. Considering the data below, a number of elements higher than five is desirable to be selected, where deviations lower than 1 % are obtained.

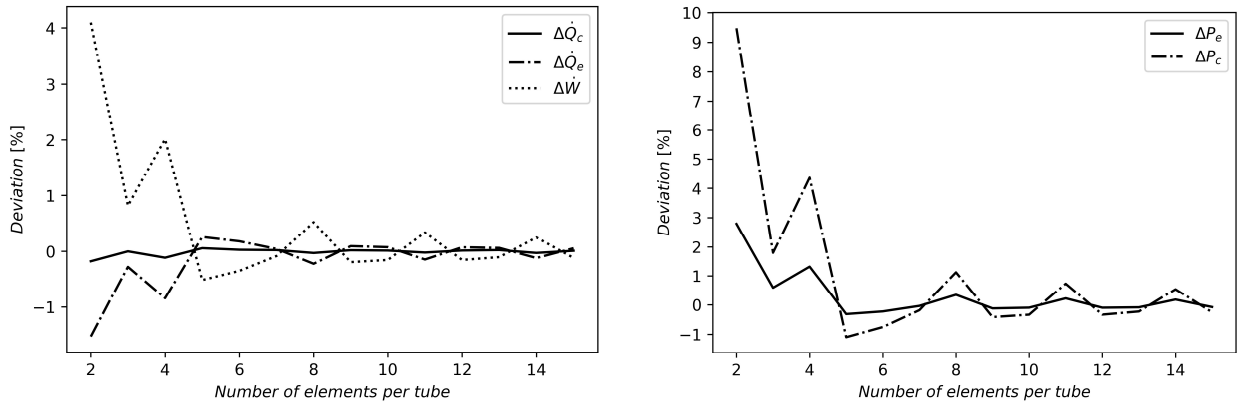

(a) Deviation on cooling capacity and compressor power (b) Deviation on working pressures

Figure 4 – Sensibility analysis of the number of elements per tube

One of the main characteristics of a hybrid vehicle is the independency of the compressor speed in relation to the engine speed, which provides opportunities for energy saving. Figure 5 shows the evaporator heat duty as a function of the compressor speed while the evaporating and condensing pressures were set to vary in order to a subcooling and superheating to be obtained. It can be noted that the total heat duty increases with an increase to the compressor speed, although part of the total heat duty corresponds to latent heat due to the decrease of the evaporating temperature and consequently increase on condensation of water vapor. From 1000 to 8000 rpm the total heat duty is about four times higher yet the sensible heat duty only doubles itself, the excess is due to the latent heat part.

It can also be seen that the ratio between the latent heat to the total heat is 0 % at 1000 rpm, goes up to 30 % at 4000 rpm and reaches a maximum of almost 40 % at the highest speed, therefore, only 60 % of the cooling capacity is accountable for the sensible heat transfer.

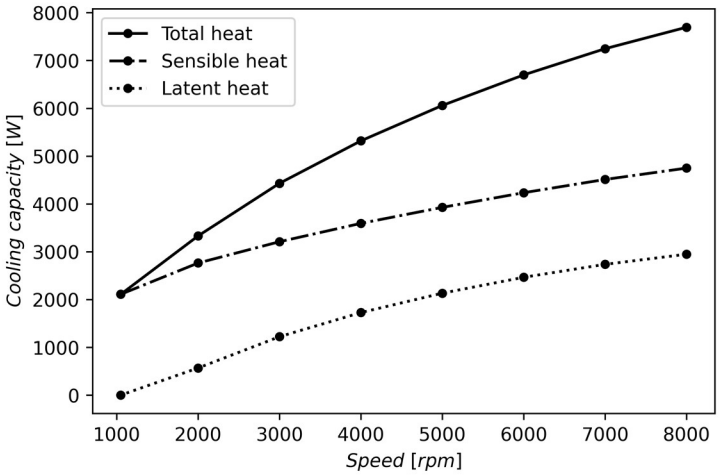

Figure 5 – Cooling capacity as a function of compressor speed

Figure 6 shows the air outlet temperature as a function of the compressor speed. As expected, the increase of the compressor speed results in a decrease of the air temperature. It is observed that the air reaches the condition of 3 °C, presented in Table 3, when the compressor speed is close to 8000 rpm.

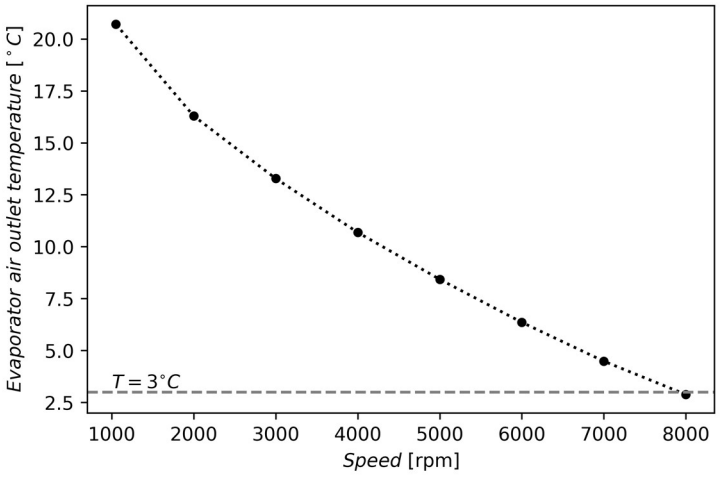

Figure 6 – Evaporator air outlet temperature as a function of compressor speed

Figure 7 shows the simulated results of heat duty ($\dot{Q}_{evap}$) power consumption ($\dot{W}_{cp}$) and COP as a function of the compressor speed. Although the evaporator heat duty increases with a higher compressor speed, the system COP decreases due to a higher increase in compressor power. At maximum speed the system can reach a COP of 2.5, which still can be considered an adequate value, with a cooling capacity of approximately 7500 W. For low speed the system can achieve COP values up to 7 although only 2000 W cooling capacity is available. Figure 7 also shows that the compressor speed has a significant impact on the system COP. For instance, a decrease from 6000 rpm to 3000 rpm

increases the COP from 2.95 to 4.45, which represents a change of 51 %. This result shows that the compressor speed control is an effective method to increase the system energy performance.

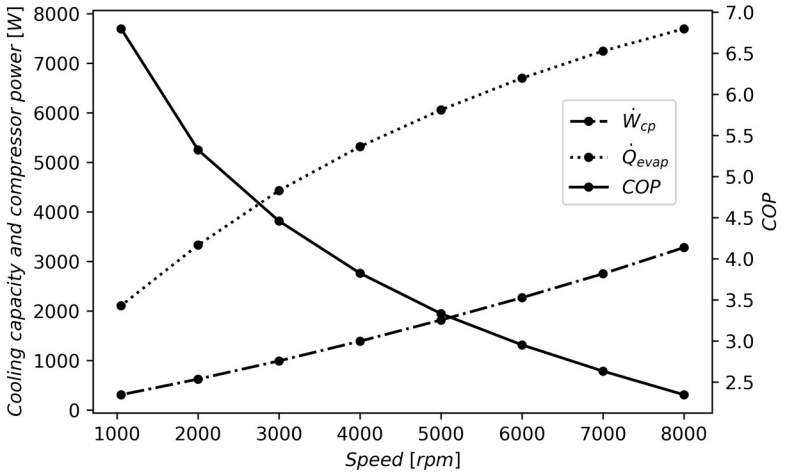

Figure 7 – Air conditioning system performance as a function of compressor speed

A common issue to the system is the presence of water vapor in the air, an excessive humidity deteriorates the sensible heat transfer accountable to reduce the air temperature in the vehicle. Such issue must be covered by the entire system considering that vehicles are susceptible to operate in any kind of conditions over its lifespan. Figure 8 shows the evaporator heat duty while the evaporating and condensing pressures were also set to vary for a compressor speed of 6000 rpm. As can be seen, the total heat duty increases with an increase in the relative humidity despite that the sensible heat transfer decreases during the process, as consequence the latent heat becomes higher while the water vapor condensation process intensifies. The latent and sensible heat duty becomes equal value for approximately 55 % relative humidity, while for 100 % relative humidity the latent heat duty is accountable for, approximately, 72 % of the total heat duty.

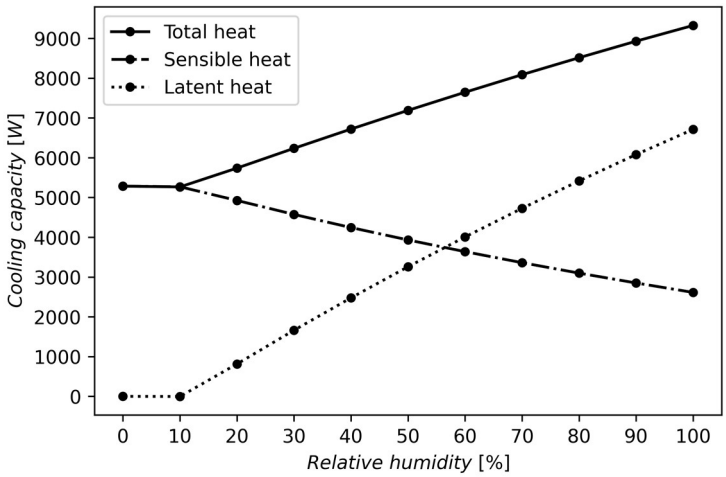

Figure 8 – Cooling capacity as a function of relative humidity

Even though the sensible heat transfer decreases with the increase in the inlet air relative humidity, the system COP increases as can be seen in Figure 9. In fact, the total heat duty becomes higher as the relative humidity increases, however, it cannot be analyzed as a separated output due to the fact that the air conditioning system must cover not only the heat duty but also the air outlet temperature.

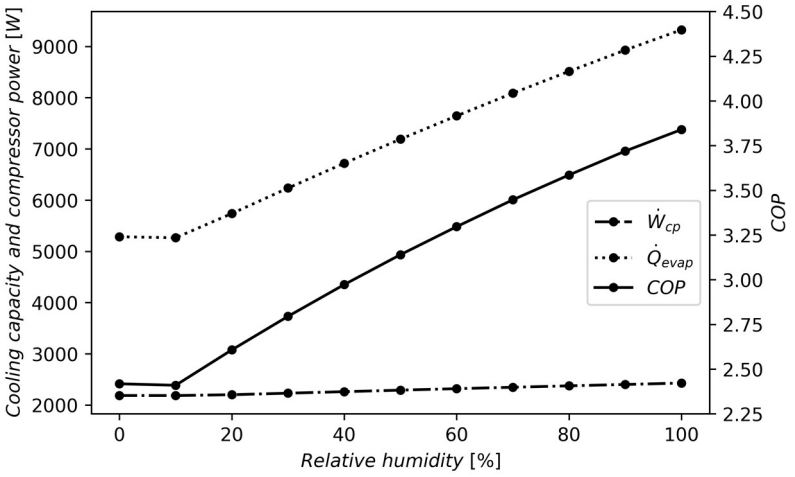

Figure 9 – Cooling capacity, compressor power and system COP as a function of relative humidity

Figure 10 shows the air outlet temperature as a function of the inlet air relative humidity for a compressor speed of 6000 rpm, is notable that a high relative humidity deteriorates the condition of the outlet air. Also, depending on the external ambient conditions and the passenger demand, the air conditioning system could not be able to achieve the required cabinet temperature. The system is capable to attend SAE J2765 (2017) conditions up to about 25 % relative humidity, higher than that the AC system considered in this study cannot achieve temperatures below 3 °C.

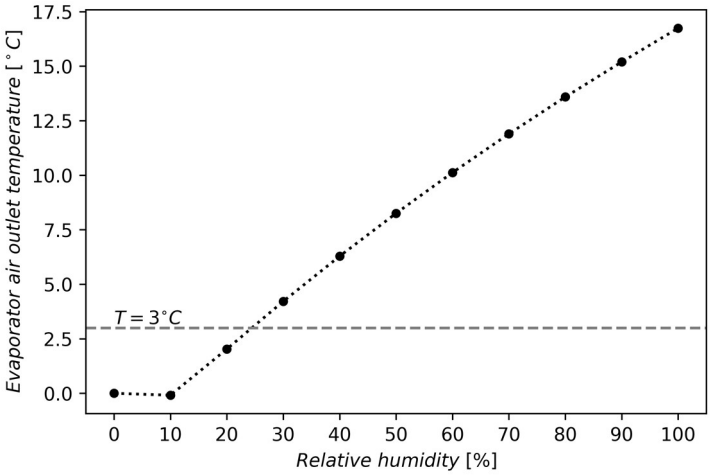

Figure 10 – Evaporator air outlet temperature as a function of relative humidity

5. CONCLUSIONS

A steady-state air conditioning system model was presented in this paper, the model was developed based on thermodynamics principles and empirical correlations. A Newton-Raphson like method was implemented to solve for the system model while a successive substitution method was used to solve for the heat exchangers discretized model. It was noted that an optimum number of control volumes per tube in the heat exchangers method can be obtained to reduce machine execution time while a proper convergence error can also be attained, a minimum of 5 elements per tube was identified as a proper value where deviations less than 1 % can be achieved.

The effect of the compressor speed on the main parameters of the air conditioning system was also investigated. The cooling capacity becomes higher as the compressor speed increases, while the system COP decreases due to the increase in compressor work power. It was observed that a decrease from 6000 rpm to 3000 rpm increases the COP by 50%, showing that the compressor speed control is an effective method to increase the system energy performance. Although the cooling capacity increases, part of the heat duty is due to the latent heat that occurs in the dehumidification process. The simulated AC system can deliver cooling capacity up to about 7500 W at 8000 rpm although only 60 % is accountable for the sensible heat transfer. Also, considering the SAE J2765 (2017) requirements, the required air outlet temperature is achieved at a compressor speed close to 8000 rpm.

Moreover, a sensibility analysis of the effect of the air inlet relative humidity was also evaluated. It was noted that as the relative humidity increases the total heat duty also increases and the system COP also increases, however, the heat increase is due to the water vapor condensation. For a high relative humidity, the latent heat is accountable for a vast part of the total heat duty, as consequence the air outlet temperature increases and might not be able to attend the air conditioning requirements. The simulated AC system, at compressor speed of 6000 rpm, was able to meet the outlet air requirements for relative humidity up to 25 %, for relative humidity higher than that the air outlet temperature was higher than 3 °C and for 100 % relative humidity the latent heat is accountable for almost 72% of the cooling capacity.

6. ACKNOWLEDGEMENTS

This work was carried out at POLO/UFSC under the auspices of the Institutos Nacionais de Ciência e Tecnologia program (CNPq 404023/2019-3, FAPESC 2019TR0846).

7. REFERENCES

Chang, Yu Juei *et al.* A generalized friction correlation for louver fin geometry. *International Journal of Heat and Mass Transfer*, v. 43, n. 12, p. 2237–2243, 2000.

Chang, Yu Juei; Wang, Chi Chuan. A generalized heat transfer correlation for louver fin geometry. *International Journal of Heat and Mass Transfer*, v. 40, n. 3, p. 533–544, 1997.

Churchill, Stuart W. Friction-factor equation spans all fluid-flow regimes. 1977.

Farrington, R.; Rugh, J. Impact of Vehicle Air-Conditioning on Fuel Economy, Tailpipe Emissions, and Electric Vehicle Range. *Earth Technologies Forum*, n. September, p. http://www.nrel.gov/docs/fy00osti/28960.pdf, 2000. Available at: <http://www.smesfair.com/pdf/airconditioning/28960.pdf>.

Feng, Lili; Hrnjak, Pega. Experimental and Numerical Study of a Mobile Reversible Air Conditioning- Heat Pump System. *International Compressor Engineering, Refrigeration and Air Conditioning, and High Performance Buildings Conferences*, p. 1–10, 2016.

Gonçalves, Joaquim M. *et al.* A semi-empirical model for steady-state simulation of household refrigerators. *Applied Thermal Engineering*, v. 29, n. 8–9, p. 1622–1630, 2009. Available at: <http://dx.doi.org/10.1016/j.applthermaleng.2008.07.021>.

IEA. Global EV Outlook 2022. 2022. Available at: <https://www.iea.org/reports/global-ev-outlook-2022>.

Kim, Sung Min; Mudawar, Issam. Universal approach to predicting two-phase frictional pressure drop for mini/micro-channel saturated flow boiling. *International Journal of Heat and Mass Transfer*, v. 58, n. 1–2, p. 718–734, 2013. Available at: <http://dx.doi.org/10.1016/j.ijheatmasstransfer.2012.11.045>.

Ko, Jaedeok *et al.* Transient analysis of an electric vehicle air-conditioning system using CO2 for start-up and cabin pull-down operations. *Applied Thermal Engineering*, v. 190, n. March, p. 116825, 2021. Available at: <https://doi.org/10.1016/j.applthermaleng.2021.116825>.

Lee, Jong Tae *et al.* Effect of air-conditioning on driving range of electric vehicle for various driving modes. *SAE Technical Papers*, v. 1, n. December 2013, p. 5–9, 2013.

Li, Wenhua. Simplified steady-state modeling for variable speed compressor. *Applied Thermal Engineering*, v. 50, n. 1, p. 318–326, 2013. Available at: <http://dx.doi.org/10.1016/j.applthermaleng.2012.08.041>.

Liang, Kunfeng *et al.* Advances and challenges of integrated thermal management technologies for pure electric vehicles. *Sustainable Energy Technologies and Assessments*, v. 46, n. January, p. 101319, 2021. Available at: <https://doi.org/10.1016/j.seta.2021.101319>.

Petukhov, B. S. Heat Transfer and Friction in Turbulent Pipe Flow with Variable Physical Properties. *Advances in Heat Transfer*, v. 6, n. C, p. 503–564, 1970.

SAE International. Procedure for Measuring System COP [Coefficient of Performance] of a Mobile Air Conditioning System on a Test Bench. *SAE Standard J2765*, 2017. Available at: <https://www.sae.org/standards/content/j2765_201707>.

Shah, Mirza M. A correlation for heat transfer during condensation in horizontal mini/micro channels. *International Journal of Refrigeration*, v. 64, p. 187–202, 2016. Available at: <http://dx.doi.org/10.1016/j.ijrefrig.2015.12.008>.

Shah, Ramesh K; Sekulic, Dušan P. *Fundamentals of Heat Exchanger Design*. . [S.l: s.n.], 2003.

Stoecker, Wilbert F. *Industrial Refrigeration Handbook*. First edit ed. New York: McGraw-Hill Education, 1998. Available at: <https://www.accessengineeringlibrary.com/content/book/9780070616233>.

Wang, Jianfeng; Hihara, Eiji. Prediction of air coil performace under partially wet and totally wet cooling conditions using equivalent dry-bulb temperature method. *International Journal of Refrigeration*, v. 26, n. 3, p. 293–301, 2003.

Zhang, Zhenying *et al.* The solutions to electric vehicle air conditioning systems: A review. *Renewable and Sustainable Energy Reviews*, v. 91, n. February, p. 443–463, 2018.

8. RESPONSIBILITY NOTICE

The authors are the only responsible for the printed material included in this paper.